

The annual cycle of Northern Hemisphere storm-tracks. Part 2: regional detail

Article

Accepted Version

Hoskins, B. J. and Hodges, K. I. ORCID:
<https://orcid.org/0000-0003-0894-229X> (2019) The annual cycle of Northern Hemisphere storm-tracks. Part 2: regional detail. Journal of Climate, 32. pp. 1761-1775. ISSN 1520-0442 doi: 10.1175/jcli-d-17-0871.1 Available at <https://centaur.reading.ac.uk/76417/>

It is advisable to refer to the publisher's version if you intend to cite from the work. See [Guidance on citing](#).

To link to this article DOI: <http://dx.doi.org/10.1175/jcli-d-17-0871.1>

Publisher: American Meteorological Society

All outputs in CentAUR are protected by Intellectual Property Rights law, including copyright law. Copyright and IPR is retained by the creators or other copyright holders. Terms and conditions for use of this material are defined in the [End User Agreement](#).

www.reading.ac.uk/centaur

CentAUR

Central Archive at the University of Reading

Reading's research outputs online



AMERICAN METEOROLOGICAL SOCIETY

Journal of Climate

EARLY ONLINE RELEASE

This is a preliminary PDF of the author-produced manuscript that has been peer-reviewed and accepted for publication. Since it is being posted so soon after acceptance, it has not yet been copyedited, formatted, or processed by AMS Publications. This preliminary version of the manuscript may be downloaded, distributed, and cited, but please be aware that there will be visual differences and possibly some content differences between this version and the final published version.

The DOI for this manuscript is doi: 10.1175/JCLI-D-17-0871.1

The final published version of this manuscript will replace the preliminary version at the above DOI once it is available.

If you would like to cite this EOR in a separate work, please use the following full citation:

Hoskins, B., and K. Hodges, 2019: The Annual Cycle of Northern Hemisphere Storm-Tracks. Part 2: Regional Detail. *J. Climate*. doi:10.1175/JCLI-D-17-0871.1, in press.



The Annual Cycle of Northern Hemisphere Storm-Tracks. Part 2: Regional Detail

B. J. Hoskins and K. I. Hodges

Department of Meteorology, University of Reading, Reading, United Kingdom.

PRELIMINARY ACCEPTED VERSION

Abstract

In Part 1 of this study, the annual cycle of the Northern Hemisphere storm-tracks was investigated using feature tracking and Eulerian variance based diagnostics applied on both vorticity and meridional wind. Results were presented and discussed for the four seasons at both upper (250hPa) and lower (850hPa) tropospheric levels. Here, using the meridional wind diagnostics, the annual cycles of the North Pacific and North Atlantic storm-tracks are examined in detail. This is done using monthly and 20° longitudinal sector averages. Many sectors have been considered, but the focus is on sectors equally spaced in the two main oceanic storm-tracks situated at their western, central and eastern regions, the western ones being mainly over the upstream continents.

The annual cycles of the upper and lower tropospheric storm-tracks in the central and eastern Pacific, and western and central Atlantic sectors all have rather similar structures. In amplitude, each sector at both levels has a summer minimum and a relatively uniform strength from October to April, despite the strong winter maxima in the westerly jets. However, high intensity storms occur over a much wider latitudinal band in winter. The storm-track in each sector moves poleward from May to August and returns equatorward from October to December, and there is a marked asymmetry between spring and autumn.

There are many differences between the North Pacific and North Atlantic storm-tracks, and some of these seem to have their origin in the behaviour over the upstream East Asian and North American continents, suggesting the importance of seeding from these regions. The East Asian storm-track near 48°N has marked spring and autumn maxima and weak amplitude in winter and summer. The 33°N track is strong only in the first half of the year. In contrast, the eastern North American storm-track is well-organised all year, around the baroclinicity that moves latitudinally with the seasons. The signatures associated with these features are found to gradually decrease downstream in each case. In particular, there is very little latitudinal movement in the storm-track in the Eastern Atlantic.

1 Introduction

The winter Northern Hemisphere (NH) storm-tracks have been the subject of many previous studies (e.g. Blackmon, 1976; Chang et al, 2002; Hoskins and Valdes, 1999; Hoskins and Hodges, 2002). In his seminal study, Nakamura (1992) presented pictures of the annual cycle of the North Pacific and North Atlantic storm-tracks based on high pass filtered variance of geopotential at 250hPa and the sea-level pressure. His focus was on the winter half of the year and he contrasted the mid-winter minimum in the Pacific with the expected winter maximum in the Atlantic. Subsequent papers, e.g. Ren et al. (2010), Penny et al., (2010), Chang and Guo (2012), Ren et al (2014), and recently Afargan and Kaspi (2017) (and also, very recently, Schemm and Schneider, (2018)) have shown annual cycles but have focussed on this winter behaviour. However, relatively little attention has been given to the NH storm tracks in other seasons or to the details of their annual cycle.

An earlier study whose results might be expected to be relevant to the storm-tracks is that of Fleming et al (1987) who considered the annual cycle of the zonally averaged westerly wind at 500hPa. The focus of Fleming et al (1987) was the asymmetry between spring and autumn, with the latitudes of the jet in spring and autumn being 33°N and 46°N, respectively. The largest amplitudes and southern-most latitudes were found to occur in mid-winter, and weakest amplitudes in July and highest latitudes in August.

This paper forms the second part of a study of the annual cycle of the observed NH storm-tracks. In Part 1 of this study (Hoskins and Hodges, 2017, hereafter HH1) high-pass standard deviation and cyclone tracking metrics were applied to vorticity and meridional wind in the upper troposphere (250hPa) and lower troposphere (850hPa) to produce the seasonal average storm tracks which were presented and discussed. Comparisons between

the results for different metrics, variables, and levels, and between the Pacific and Atlantic storm-tracks were made. Amongst the results it was found that the North Pacific upper tropospheric storm-track is indeed weaker in winter than in autumn or spring when viewed using high-pass standard deviation of both variables, but with tracking measures and in the lower troposphere this minimum was less marked. The seasonal positions of the storm-tracks were in general found to be qualitatively consistent with that of the zonally averaged jet found by Fleming et al (1987). However, these and other aspects would benefit from a more detailed view of the annual cycle. This is the motivation for this second paper in which the annual cycle of the two major Northern Hemisphere storm-tracks, the North Pacific and the North Atlantic storm-tracks are examined in detail using averages over particular, representative longitudinal sectors and for the calendar months. The primary motivation for this paper and its companion is to further the basic understanding of storm-tracks and the ability to diagnose the storm-tracks in climate models. It is not directly aimed at the impacts associated with storms, though this is of course an important area for study.

Sector averages have been used by a number of authors in order to summarise the storm-track behaviour in broad regions. For example, Nakamura (1992) used 60° sectors in the Pacific and the Atlantic, and Penny et al (2010), and Afargan and Kaspi (2017) used 40° sectors. These sector widths were satisfactory for the topics considered, but it is clear from the geographical storm-track pictures shown in HH1 that the storm-tracks in some regions can vary significantly over such longitudinal ranges. In particular averages over a broad range of longitudes are problematic for a south-west to north-east tilted storm-track like the North Atlantic in winter. Here we will use narrower 20° sectors in order to obtain a more local picture of the storm-track behaviour. The 37 years of reanalysis data used here is

sufficient that results for such narrow sectors based on diagnostics of meridional wind generally show coherent behaviour from month to month in the annual cycle.

Previous studies showing the annual cycle, e.g. Nakamura (1992), Nakamura and Sampe (2002), Ren et al. (2010), Chang and Guo (2012) and Afargan and Kaspi (2017), have mostly used a high pass variance measure for the storm-track. However, Penny et al (2010) showed the results from both variance and feature tracking, but focussed on the tracking results. (Very recently, Schemm and Schneider, 2018, have tracked surface cyclones and used variance measures in the free atmosphere.) Here both storm-track metrics will be given equal weight in the discussion. Following Nakamura (1992), the high pass variance technique has mostly been applied to geopotential at an upper tropospheric level, but Ren et al. (2010) applied it to meridional wind at an upper tropospheric level. Nakamura (1992) also presented the annual cycle for the variance of mean sea level pressure but there has been limited discussion of lower tropospheric metrics. In this paper equal weight will be given to high-pass variance and feature tracking measures. The same metrics applied to an upper tropospheric level, 250hPa, and a lower tropospheric level, 850hPa, will be discussed for each sector. The main results presented here will be for meridional wind, V . Those obtained using vorticity are generally found to be similar.

The paper continues in Section 2 with a brief discussion of the data and methodologies used. Section 3 presents the results in separate sub-sections for the North Pacific, North Atlantic and Mediterranean, and Section 4 gives some concluding comments.

2 Data and methodology

The data and basic methodology are the same as in HH1, where full details are given. The basic data source is the European Centre for Medium-Range Weather Forecasts (ECMWF) Interim reanalysis (ERA-I) (Dee et al, 2011) for the years 1979 to 2016. The data used in this study is the 4 times per day meridional wind, V , on the 850 and 250hPa levels.

Two approaches to diagnosing the storm-tracks are employed. The first is based on the 2-6 day band-pass filtered variances (Blackmon, 1976), presented in terms of the Standard Deviation (SD). The second approach uses objective feature tracking as in the NH winter study of Hoskins and Hodges (2002), and is the same as used in HH1, where more details can be found. As in HH1, the diagnostics are performed at 250hPa, representing the upper troposphere, and 850hPa, representing the lower troposphere. In HH1 the tracking results were presented for extrema in two fields, vorticity and the modulus of meridional wind, $|V|$. In HH1 a detailed discussion of using the latter and the relative advantages of the two variables is given. The latter is equivalent to tracking both positive and negative extrema in V and combining the results. Briefly, the justification for using $|V|$ is that the growth of storms depends on both warm air moving polewards and cold air moving equatorwards, and in addition tracking $|V|$ provides the best comparison with the band-pass SD of V , which also makes no discrimination between signs. In this paper, SD of V and tracking of $|V|$ will be used instead of vorticity as the finer scales described by vorticity sometimes lead to some lack of continuity between months in sectors as narrow as the ones used here. Tracking has also been performed separately for positive and negative V extrema and these results will be mentioned in cases where this detailed additional information is of interest.

The sectors in which the storm-tracks are to be studied in detail are shown in Figure 1. This shows the December-February (DJF) winter-time cyclone track density and mean intensity for maxima in the modulus of the meridional wind at 850hPa (V_{850}), similar to Figure 10a of HH1. As discussed in detail there, the North Pacific and North Atlantic storm-tracks are clearly delineated at this level. The sectors have been chosen to sample the western/upstream, central and eastern/downstream regions of the two main storm-tracks. They are all 20° in longitude, with three equally spaced (with 30° separation) in the Pacific storm-track and three equally spaced (with 10° separation) in the Atlantic storm-track. The sectors are: West Pacific (WP: 110E-130E), Central Pacific (CP: 160E-180E), East Pacific (EP: 150W-130W), West Atlantic (WA: 80W-60W), Central Atlantic (CA: 50W-30W), East Atlantic (EA: 20W-0W). The nomenclature, West, Central and East are with reference to the relevant storm-track and not the ocean basin. For example, in the latitudes of interest, the WP sector is mainly in East Asia, and WA is more in North America than over the Atlantic. To understand the context further upstream and the continuity between sectors, results from a number of other sectors have been computed and considered. Sectors further west over Asia (100°E-120°E) and over North America (90°W-70°W) are shown in the Supplementary Material. Also shown there are the results for a 10°E-30°E sector that gives a picture of the seasonal cycle of the Mediterranean storm-track. In addition it shows the extension of the North Atlantic storm-track into Europe, though the interruption of the 850hPa surface by the Alps should be noted as giving a region of doubtful validity of the diagnostics between the two storm-track regions. The borders of the three sectors shown in the Supplementary Material are indicated by yellow lines in Figure 1.

In the following Section, the North Pacific storm-track will be discussed first, starting with the CP sector, motivated by the previous interest in the mid-winter minimum in the Pacific.

3 Results

3.1 The North Pacific

3.1.1 The Central Pacific (CP)

The CP sector zonal mean of SD of the band-pass V at both 250hPa and 850hPa are shown as functions of time of year (abscissa) and latitude (ordinate) in Figures 2a, c. The January to December period is continued by a repetition of the 6 months of January to June, so that the annual cycle is clear throughout the year. Overlain on the SD panels are contours of a relevant zonal wind, U . At 250 hPa, U is shown on the dynamical tropopause (the $PV=2$ surface, see e.g. Hoskins (2015)) and highlights both the sub-tropical and polar jets. This is used because of its theoretical importance for developments in the upper troposphere in general (see e.g. Hoskins and James, 2014). However, U on the 250hPa level (not shown) itself is very similar, showing jets at the same latitudes with only slightly smaller strengths. At 850 hPa, the zonal wind at that level is used. Figures 2b, d give the track density (line contours) and mean intensity (filled colour contours) for $|V|$ maxima at the same upper and lower tropospheric levels.

In the CP, the SD at both levels (Figures 2a, c) is dominated by the middle latitude storm-track, and shows its annual cycle in amplitude and latitude. The mid-winter minimum is apparent in both the upper and lower troposphere, though much less so at the lower (850hPa) level. This contrasts with the winter maximum in U at both levels. A marked mid-summer minimum in SD, as well as in U , is apparent at both levels. It is also clear that the autumn maxima are further poleward than those in spring.

The tracking panels (Figures 2b, d) give a more complex picture. In the upper troposphere, the track density (Figure 2b) shows spring and autumn maxima. The mean intensity is large in the autumn storm-track, but in mid-winter the higher intensity values

are less confined to the region of high track density, with the highest values found at even lower latitudes than the track density maximum. In spring, the maximum intensities are back in the storm-track, but there is now a secondary maximum at low latitudes. The mid-winter minimum in SD is therefore a reflection of both fewer storms and reduced intensities in the main storm-track region. However there are strong storms with tracks over a wide range of latitudes.

The tracking picture is again simpler in the lower troposphere (Figure 2d) with the highest intensities in the storm-track region throughout the year. Here, the overall impression is of a single extended maximum from September to May. The weak mid-winter minimum in SD is related to slightly weaker mean intensities in the storm-track region. However, at that time the region of high intensities also spreads in latitude, this time particularly on the poleward side.

The almost straight bounding contours on the poleward side of the 850 hPa track density for the main storm-track imply that it stays equatorward of the Kamchatka Peninsula all year. At both levels there is also a polar, Arctic maximum in track density in the summer time (Serreze and Barrett, 2008). At 850hPa, this leads to a weak maximum in SD (Figure 2b) there, but the more prominent Arctic maximum in SD is in winter, associated with the larger intensities at that time of year (Zhang et al., 2004)

At both levels and in both measures, the major storm-track movement in latitude largely reflects that of the zonal wind, with the upper tropospheric storm-track slightly poleward of the maximum in the westerlies. However, in the upper troposphere in winter the relationship is less definite. The SD maximum does not move as far equatorward as that in

U. The track density maximum is north of the jet but the storms with highest mean intensity are slightly south of the jet.

To study in more detail the annual cycle in the main storm-track, the latitude (ordinate) of the SD maximum and the amplitude (abscissa) of the maximum in each month are shown in Figures 3a and c, respectively for the two levels. The months are shown as dots with different colours and the annual cycle is made clearer by lines joining successive months, starting at January and finishing at December. In the upper troposphere (Figure 3a), the mid-winter minimum is apparent in that the March, April and May, and October and November amplitudes are all slightly higher than those in January and February when the storm-track is at relatively low latitudes.

The annual cycle shows a poleward shift and growth from February to March, a sharp decrease in amplitude from May to June, a poleward shift through July to August, a shift equatorward by September and growth that continues into November followed by a further equatorward shift and reduction in amplitude through December to January. Figure 3c shows that at 850hPa the mid-winter shift equatorward to below 40°N does not occur and the mid-winter minimum is less marked, with the amplitude being similar over the extended winter from October to April. As in the upper troposphere, minimum values again occur from June to August and this is the period of the main poleward shift. The main increase in amplitude occurs from then until October and the main decrease in latitude from November to December. The hysteresis-like curves at both levels clearly illustrate the asymmetry between spring and autumn.

It is of interest to obtain similar annual cycle summaries for the main storm-track using the tracking of $|V|$. In each month the track density shows a relatively sharp maximum, but

the mean intensities have a broader distribution. Therefore it has been decided to identify the latitude of the storm-track by the track density maximum, and use the mean intensity at that latitude as the measure of strength, with these two acting as the descriptors of the storm-track behaviour for each month. This gives the annual cycle summary pictures in Figures 3b and d for the two levels. The behaviour at both levels is generally similar to that shown for the SD in Figures 3a and c. Again apparent are: the January-February equatorward displacement with a minimum in amplitude at both levels, low intensities and a poleward shift in the period June-August, and a latitude difference between spring and autumn, with the spring latitude closer to that of winter and the autumn storm-track latitude closer to that of late summer. With this diagnostic, the mid-winter minimum is apparent at 850hPa as well as 250hPa.

It is of interest to note that in this sector, the large sea surface temperature gradients associated with the extension of the Kuroshio are in the latitude band 30°N-40°N, and only the winter storm-track can be affected directly by them.

3.1.2 West Pacific (WP)

The WP sector has its own intrinsic interest. In addition there has been much discussion (e.g. Hakim, 2003; Orlanski, 2005; Chang, 2005; Robinson, 2006; Penny et al., 2010; Chang and Guo, 2012) of the seeding from the WP of the storm-track in the CP, in particular in its possible importance in the mid-winter minimum there. The Kuroshio occurs only in the easternmost part of this 20° sector and then with a south-north orientation. The zonal averages in the WP sector are not designed to diagnose the impact of the Kuroshio and in any case the scale resolved by the data used is probably not suitable for this.

Figure 4 shows the WP sector average SD and tracking results at the two levels. The SD results (Figures 4a, c) for the main storm-track are generally weaker versions of those for the CP (Figures 2a, c). However, in this sector the mid-winter minimum in the upper troposphere is almost as marked as the mid-summer minimum. The upper tropospheric tracking diagnostics (Figure 4b) are also similar to those for the CP (Figure 2b), except that the mean intensities are weaker and the mid-winter minimum is more evident in both track densities and intensities. The behaviour is largely decoupled from that of the jet (Figure 4a) except that there is an intensity maximum that is coincident with the winter jet maximum.

There are indications of a more complex structure in the lower tropospheric SD (Figure 4c). In Spring there are signs of separate maxima near 45°N and 30°N , and in Spring and Autumn also maxima near 65°N . In the tracking results (Figure 4d) these features become more apparent. In the latitudes 30° - 50°N the track density exhibits a double structure in latitude. The northern maximum, centred on 48°N , is present most of the year, and is prominent from March to June and August to December. Its importance for the Pacific storm-track has been discussed by Nakamura (1992), Hakim (2003), Orlanski (2005), Chang (2005), Penny et al. (2010), and Chang and Guo (2012). The southern maximum, centred on 33°N , is present only in the first half of the year, and is prominent from February to May. Nakamura and Sampe (2002) mentioned the possible importance for the Pacific storm-track of waves on this southern branch, and Chang (2005) gave evidence of constructive interference between wave packets on the two tracks.

Associated with the 850 hPa double track in spring and the single track in autumn, there are weak maxima in the westerly winds at the same level (Figure 4c). In the autumn the northern track is prominent at both levels in both track density and SD (Figure 4), so that the

systems are vertically deep. However, in the spring the upper tropospheric track is centred between the two lower tropospheric tracks, so that a linkage with either is possible. This behaviour contrasts with that in the CP where the upper and lower tropospheric track densities are coherent throughout the year. The two tracks in WP can be seen in the winter and spring 850hPa tracking pictures given in HH1 for meridional wind (Figure 10a, b) and positive vorticity (Figure 7a, b). For winter, the northern track is the south-eastward extension of the Siberian track discussed by Wallace et al. (1988) and the southern one, in the region of the sub-tropical jet, was highlighted by Chang and Yu (1999). Later in the year, the latter corresponds to the Spring Persistent Rains in China discussed by, for example, Tian and Yasunari (1998). The possible importance of the WP behaviour for that in CP will be discussed further in Section 4.

Also clearly marked in the 850hPa tracking results (Figure 4d) is a maximum in track density near 65°N from March to October with a weak minimum in mid-summer. The mean intensities emphasise the spring and autumn periods, making this storm-track feature consistent with the signatures near 65°N commented on above. Looking again at Figure 4b, similar features are also apparent in the 250hPa tracking results. The features are even clearer in the 100E to 120E sector shown in Figure S1. Referring to Figures, 7, 8, 10 and 11 of HH1, the presence of the 850hPa eastward extension near 65°N from the Siberian storm-track to 110E-120E is clear in both vorticity and meridional wind, and in both SD and tracking. However, in the upper troposphere the track leading south-east towards the region of the 48°N lower troposphere track is dominant.

Near 15°-20°N, the May-November maximum in track density (Figures 4b, d) is more marked at both levels than in the CP, and is the signature of westward moving Western

Pacific tropical cyclones. At 850hPa the track density maximum is accompanied by large mean intensities and so the signature is seen also in the SD (Figure 4b).

3.1.3 East Pacific (EP)

Moving eastwards from the CP, the EP SD and tracking results at the two levels are shown in Figure 5. The main storm-track in the upper troposphere (Figures 5a, b) again exhibits a mid-winter minimum in SD and in track density. In mid-winter the spread of larger SD values to lower latitudes is associated with a secondary maximum in track density accompanied by high intensities. This is the signature of the cut-off lows, the “subtropical cyclones” whose surface features are referred to as Kona lows and that have been discussed by, for example, Simpson (1952), and Otkin and Martin (2004). The high intensities at low latitudes seen in CP in the winter (Fig. 2b) may also reflect such features.

In the lower troposphere (Figure 5c, d) both the SD and track density give a slight emphasis to the first half of winter. The mid-winter expansion to lower latitudes is again apparent in the tracking fields (Figure 5d). At this lower level, the storm-track in this sector is bounded near 58°N at all times of the year by the southern coast of the Alaskan Peninsular. At low latitudes the track density signature of westward moving Eastern Pacific tropical cyclones is seen from June to October. In high latitudes the track density again has a summer maximum in the Arctic, off the northern coast of Alaska, but it is the winter intensity maximum that is picked up more strongly by the SD.

At both levels, the westerly winds themselves show a slight winter minimum in this sector. The storm-tracks and the winds tend to move together through the annual cycle,

with the storm-track slightly poleward of the maximum winds except for the upper troposphere from January to April.

Figure 6 shows the EP annual cycle summaries for SD and tracking and for the two levels using the same format as for CP in Figure 3, and the results are quite similar to those. All four panels show a fairly flat maximum from October to April with the actual peak mostly in December. Each then shows a strong reduction in magnitudes to those of the summer, this being about 50% at the lower level. Each also show a lower latitude for the storm-track in winter and early spring, and a higher latitude in late summer and early autumn. This asymmetry between spring and autumn is again marked.

3.2 The North Atlantic

3.2.1 West Atlantic (WA)

As seen in Figure 1, the WA sector includes eastern North America. The Gulf Stream is present at the eastern portion of the sector, moving from near 30°N to near 40°N across the sector. As with the case of the WP, the zonal average in the sector will not, and is not intended to capture the details of the atmospheric interaction with the Gulf Stream.

The WA sector average annual cycle results are given in Figure 7. In the annual cycle, the track densities (Figures 7b, d) have a weak summer maximum but show less variation in amplitude through the year than in the CP and EP. The mean intensities are a maximum in the winter half of the year and lower in the summer. The latter is reflected in minima in the SD results (Figures 7a, c) in summer, but these minima are not as marked as in the Pacific. The upper tropospheric mean intensity (Figure 7b) again spreads to lower latitudes in winter, but with the low number of tracks this is only weakly reflected in SD (Figure 7a), and

is not as prominent as in the CP and EP. The signature of westward moving Atlantic tropical cyclones is apparent in all the panels from June to October.

As in the CP, the upper tropospheric westerly winds are strongest in mid-winter (Figure 7a). However, unlike the Pacific, the jet continues to move slightly equatorward until March. In the upper troposphere in April-May a second westerly maximum appears some 15° further north, and it is the northern maximum that continues through the summer, moving slowly poleward. The storm-track in all measures is poleward of the strongest westerlies, with the displacement becoming large as the westerly jet continues to move equatorward after January.

Figure S2 in the Supplementary Material, shows results for the sector centred 10° further west. Results have also been obtained for a sector 10° further east (not shown). The storm-track diagnostics are all very similar but with slightly reduced SD amplitude and track mean intensities to the west which increase to the east.

Summaries of the annual cycle in the latitude and strength of the middle latitude storm-track for the WA sector are given in Figure 8. At 250hPa (Figures 8a, b) the storm-track is furthest equatorward in February, near 40°N , and furthest poleward in August-September, near 50°N , much as in the Pacific. The amplitude varies little in the period September to May with a weak maximum in November. The minimum occurs in July and August, but the summer reduction is smaller than in the Pacific. A significant poleward shift does not occur until May or June and the return to lower latitudes does not occur until October or November. The 850hPa results (Figures 8c, d) are similar, showing loops from low latitudes and high amplitudes in the period November to April and high latitudes and low amplitudes in July and August, with the early summer and autumn changes occurring first in amplitude.

In the lower troposphere the amplitude range is only slightly less than in the Pacific. In all the diagnostics, the latitude of the storm-track changes little from December to April, the period when the upper tropospheric jet is still moving slowly equatorward. As discussed in HH1, it is only in this period that the storm-track is close to the region of strong Gulf Stream SST gradients.

3.2.2 Central Atlantic (CA)

The CA sector average annual cycle results are presented in Figure 9. There are again considerable similarities with the WA (Figure 7), though the amplitudes of the SD (Figures 9a, c) and the mean intensities (Figures 9b, d) are slightly larger at both levels, and the latitude ranges in the annual cycles are somewhat smaller. The summer minima in SD at the two levels are even less marked than in the WA. This is associated with a stronger summer maximum in track density at both levels.

The two levels also have secondary maxima in track density in winter. In the lower troposphere (Figure 9d) this is quite strong and the definite mid-winter maximum in SD is consistent with this. In the upper troposphere, the winter maxima in track density (Figure 9b) and in SD (Figure 9a) is weak and the main impression is of little change in SD strength from October to March.

In the upper troposphere the large intensities again extend to lower and higher latitudes, even slightly more than in the WA. The northern side of the 850hPa storm-track (Figure 9d) is bounded by Greenland throughout the year.

As in the other sectors it is only during the extended winter period that the storm-track is at sufficiently low latitude to be directly affected by the stronger sea surface temperature

gradients near 40°N in the extension of the Gulf Stream. Afargan and Kaspi (2017) have recently discussed the existence of a winter minimum in the Atlantic storm-track, particularly in strong jet years. The diagnostics presented here for sectors from 90°W to 30°W emphasise rather that the intensity of the storm track changes little over the extended winter season.

3.2.3 East Atlantic (EA)

For the EA sector (which includes part of Western Europe), the 250hPa annual cycles in sector average storm-track measures are presented in Figure 10. In addition to the relatively weak polar jet, the tropopause zonal wind in this sector (Figure 10a) shows the sub-tropical jet over the winter half of the year. The polar jet is seen also at 850 hPa (Figure 10c), and at both levels it is near 50°N in June and, surprisingly, moves slightly north through the summer and stays there until its weakening at the end of winter. At both levels it is weakest in April and May.

In the extended winter season, September to March, the SD storm-tracks at the two levels show little change in latitude or magnitude. At both levels, the tracks have a broad distribution in latitude, centred slightly south of the jet in the upper troposphere and north of the jet in the lower troposphere. There are weak maxima in November and January. The weaker, more compact summer storm-track shows a slight poleward progression, keeping its relationship to the jet. In the EA, the SD storm-track at the two levels show remarkably little change of latitude with time of year, particularly in the extended winter season from September to March. Throughout the year the lower tropospheric storm-track is centred about 5° north of that in the upper troposphere.

The track densities (Figures 10b, d) also show a broad structure and latitudinal movement is generally small but, in concert with the jet, there is a slight poleward progression through the summer. The 250 hPa track density shows a strong summer maximum as in the CA, but is quite uniform through the rest of the year. The mean intensities have annual cycles similar to the other Atlantic sectors. Again it is the larger winter mean intensities that are reflected in the SD pictures. In the EA, the high intensities at 250 hPa spread deep into the sub-tropics and into the region of the subtropical jet from October to May. At both levels the higher intensities also spread into the polar region except in the summer.

The highest contour in track density at 850 hPa (Figure 10d) indicates a rather flat distribution with latitude from September to March, with a hint of a double maximum from November to March. The detailed monthly latitudinal profiles of track density at 850 hPa (not presented), show that for eight months of the year, November to May and also September, there are indeed two weak maxima, near 54°N and 62°N. Further investigation using the tracking of positive and negative V separately shows that the northern maximum is predominantly associated with southerly winds and the southern maximum with northerly winds.

The track densities at 850hPa also show a marked track density maximum near 20°N from May to September indicative of the African Easterly waves in this sector (Thorncroft and Hodges, 2001). The similar signature seen in Figure 9 for the CA sector marks a continuation of these, with some becoming the tropical cyclone signature in the WA (Figure 7).

4 Discussion

The focus for this study is the Pacific and Atlantic storm-tracks and these will be the subject of the discussion in this section. However, some discussion of the findings relevant to the Mediterranean storm-track, sub-tropical easterly waves and Arctic storm-tracks are given in the Supplementary Material, in sections SM.2, SM.3 and SM.4, respectively.

For the two major mid-latitude storm-tracks, the diagnostics presented here show many similarities in behaviour from one sector to another over much of the Pacific and the Atlantic, despite differences in detail. The annual cycles for the CP, EP, WA and CA in both the upper and lower troposphere have significant similarities in behaviour. In amplitude (both of SD and mean intensity from tracking), each has a summer minimum and a relatively flat distribution from October to April. The latter occurs despite the strong winter maxima in the westerly jets. The ubiquity of this result gives a more general basis for a theoretical discussion of the relationship between jets and storm-tracks in winter than the more usual focus on the mid-winter minimum in the Pacific. This discussion will have to take into account stability limitations in a strong jet (e.g. Nakamura, 1992; Christoph et al., 1997; Chang, 2001; Deng and Mak, 2005; Nakamura and Sampe, 2002; Chang and Zurita-Gotor, 2007) and other processes, such as the varying contribution from diabatic heating (Nakamura, 1992; Chang, 2001; Chang 2009).

In the winter, the storm-track structures are less coherent with the region of large storm intensities extending in latitude outside the region of maximum track density. In particular, in the upper troposphere high intensity storms are found in quite low latitudes in the central and eastern ocean basins. In Section 3.1.3 these have been identified with cut-off lows, and this identification may be applicable more generally.

Each storm-track shows a poleward movement from May to reach near 50°N in August and from October to December a return to near 40°N. Consequently, the autumn storm-track is poleward of that in spring, consistent with the asymmetry in the zonally averaged wind discussed by Fleming et al (1987).

However, there are also significant quantitative differences between the two storm-tracks. A hypothesis raised from the present work is that the upstream seeding from East Asia and North America is the origin of many of these differences. The importance of upstream seeding for the Pacific storm-track has been the subject of many earlier studies, e.g. Nakamura (1992), Hakim (2003), Orlanski (2005), Chang (2005), Robinson (2006), Penny et al. (2010), and Chang and Guo (2012). Over East Asia the south-west extension of the upper tropospheric Siberian storm-track to near 48°N where there is underlying baroclinicity downstream of the northern side of the Tibetan Plateau leads to storm-track activity with maxima in the spring and autumn seasons which are not dominated by winter or summer monsoons. The dominance of spring and autumn maxima in the storm-tracks weakens downstream, with winter values becoming more comparable, but can still be detected in the East Pacific. The summer minimum is marked along the whole storm-track.

The possible importance of the East Asian maximum in storm activity near 33°N between 100°E and 130°E has been discussed by Hakim (2003) and Chang (2005). In this paper it has been seen that the lower tropospheric maximum in track density is present only in the first half of the year, and is likely to be related to the Spring Rains in Central China. It may be linked to the subtropical jet, though the upper tropospheric maximum that is very clear in vorticity tracking (HH1, Figure 1) is situated slightly north of it. The signature of this

maximum disappears by about 150°E, though as discussed by Chang (2005) there may be interaction with storms on the more northerly track.

Turning to the Atlantic, in the sectors over eastern North America, the summer amplitude minima are less pronounced than in the Pacific sectors. In fact the track density shows a marked peak in summer. Also in the upstream sectors, the strength of the storm-track, as given for example by SD, is quite flat from October to April. In addition, there is a marked latitudinal movement in the annual cycle. These features link closely to the annual cycle in the latitude and magnitude of the baroclinicity over the North American continent. The relative weakness of the summer minimum, with a maximum in track density at that time, and the flatness of the strength in the extended winter period are found downstream along the Atlantic storm-track. The magnitude of the latitudinal cycle decreases to near zero at the eastern end of the track, implying an annual cycle in the meridional tilt of the storm-track, from SSW-NNE in the winter to almost zonal in the summer.

The track density at 250 hPa in the Pacific has a minimum in mid-winter, whereas that at 850hPa has a weak maximum then. This trend with height is consistent with the very recent paper of Schemm and Schneider (2018), where it was found that surface cyclones have a track density maximum in the mid-winter. In the Atlantic at 250hPa, there is little change in the track density over the extended winter, but 850hPa shows a weak mid-winter maximum as in the Pacific.

The annual cycle of the pdfs of lifetimes of the tracked features (not shown) have a similar behaviour in the Pacific and Atlantic, and at 250hPa and 850hPa. In each case there is a 3-day peak which is largest in winter and smallest in summer. In contrast, for life-times longer than 6 days, the summer is dominant and the winter weakest. This is consistent with

the longer periods in summer found for the Pacific by Chang and Yu (1999) and also for surface cyclones in Schemm and Schneider (2018). It is also consistent with the more marked summer minima generally seen here in the 2-6 day band pass SD pictures than in the tracking pictures.

There are many aspects of the rich Northern Hemisphere storm-track behaviour that have been shown in HH1 and here that are not well-understood, and it is hoped that these papers will provide a stimulant for further diagnosis of observations and theoretical understanding of storm-tracks. An important extension of the present study will be to consider the inter-annual variability of the seasonal cycles of the storm-tracks and the relationship with low frequency variability, in particular that associated with El Niño–Southern Oscillation (ENSO), North Atlantic Oscillation (NAO), Pacific Decadal Oscillation (PDO) and Atlantic Multi-decadal Oscillation (AMO). It is also hoped that this pair of papers provides a basis for more detailed evaluation of the performance of climate models in today’s climate and diagnosis of their projections of storm-tracks in a changing climate.

Acknowledgements

We thank Tim Woollings for provoking us into extending our previous analysis of NH storm-tracks into other seasons. We also thank Paul Berrisford and the ECMWF Reanalysis team for the provision of the basic data used in this paper. Finally, we than the Reviewers for their helpful comments.

References

- Afargan, H. and Y. Kaspi, 2017: A mid-winter minimum in midlatitude storm-track intensity in years of a strong jet. *Geophys. Res. Lett.*, doi: 10.1002/2017GL075136
- Alpert, P., and B. Ziv , 1989: The Sharav Cyclone: Observations and some theoretical considerations, *J. Geophys. Res.*, **94**, 18495–18514.
- Alpert, P., B.U. Neeman, and Y. Shayel , 1990: Climatological analysis of Mediterranean cyclones using ECMWF data, *Tellus A*, **42**, 65–77.
- Blackmon, M. L., 1976: A climatological spectral study of the 500mb geopotential height of the Northern Hemisphere, *J. Atmos. Sci.*, **33**, 1607–1623.
- Chang, E. K. M., 2001: GCM and observational diagnoses of the seasonal and interannual variations of the Pacific storm track during the cool season. *J. Atmos. Sci.*, **58**, 1784–1800.
- Chang E. K. M., S. Y. Lee and K. L. Swanson, 2002: Storm track dynamics, *J. Clim.*, **15**, 2163–2183.
- Chang E. K. M., 2005: The impact of wave packets propagating across Asia on Pacific cyclone development. *Mon. Wea. Rev.*, **133**, 1998–2015.
- Chang E. K. M., 2009: Diabatic and orographic forcing of northern winter stationary waves and storm tracks. *J. Climate*, **22**, 670–688.
- Chang, E. K. M., and D. B. Yu, 1999: Characteristics of wave packets in the upper troposphere. Part I: Northern Hemisphere winter. *J. Atmos. Sci.*, **56**, 1708–1728.
- Chang E. K. M. and P. Zurita-Gotor, 2007: Simulating the seasonal cycle of the Northern Hemisphere storm tracks using idealized nonlinear storm-track models. *J. Atmos. Sci.*, **64**, 2309–2331.
- Chang, E. K. M., and Y. Guo, 2012: Is Pacific storm-track activity correlated with the strength of upstream wave seeding?, *J. Climate*, **25**, 5768–5776.

540 Christoph, M., U. Ulbrich, and P. Speth, 1997: Midwinter suppression of Northern
 541 Hemisphere storm track activity in the real atmosphere and in GCM experiments, *J. Atmos.*
 542 *Sci.*, **54**, 1589–1599.
 543 Deng, Y., and M. Mak, 2005: An idealized model study relevant to the dynamics of the
 544 midwinter minimum of the Pacific storm track, *J. Atmos. Sci.*, **62**, 1209–1225.
 545 Fleming, E. L., H. G.-Lim, and J. M. Wallace, 1987: Differences between the spring and
 546 autumn circulation of the Northern Hemisphere, *J. Atmos. Sci.*, **44**, 1266–1286.
 547 Hakim, G. J., 2003: Developing wave packets in the North Pacific storm-track. *Mon. Wea.*
 548 *Rev.*, **131**, 2824–2837.
 549 Hannachi, A., A. Awad, and K. Amma, 2011: Climatology and classification of Spring
 550 Saharan cyclone tracks, *Clim. Dynam.*, **37**, 473–491.
 551 Hoskins, B. J. and K. I. Hodges, 2002: New perspectives on the Northern Hemisphere winter
 552 storm tracks. *J. Atmos. Sci.*, **59**, 1041–1061.
 553 Hoskins, B. 2015: Potential vorticity and the PV perspective, *Adv. Atmos. Sci.*, **32**, 2-9.
 554 <https://doi.org/10.1007/s00376-014-0007-8>
 555 Hoskins, B. J. and K. I. Hodges, 2017: The Annual Cycle of Northern Hemisphere Storm-
 556 Tracks. Part 1: Seasons, submitted.
 557 Hoskins, B. J., and P. J. Valdes, 1990: On the existence of storm-tracks. *J. Atmos. Sci.*, **47**,
 558 1854–1964.
 559 Nakamura, H., 1992: Midwinter suppression of baroclinic wave activity in the Pacific, *J.*
 560 *Atmos. Sci.*, **49**, 1629–1642, doi: 10.1175/1520-0469.
 561 Nakamura, H., and T. Sampe, 2002: Trapping of synoptic-scale disturbances into the North-
 562 Pacific subtropical jet core in midwinter, *Geophys. Res. Lett.*, **29**, 1761.

563 Orlanski, I., 2005: A new look at the Pacific storm track variability: Sensitivity to tropical SSTs
 564 and to upstream seeding. *J. Climate*, **18**, 1367–1390.

565 Otkin, J. A., and J. E. Martin, 2004: A synoptic-climatology of the subtropical Kona
 566 storm. *Mon. Wea. Rev.*, **132**, 1502-1517.

567 Penny, S., G. Roe, and D. Battisti, 2010: The source of the midwinter suppression in
 568 storminess over the North Pacific, *J. Climate*, **23**, 634–648.

569 Ren, H.-L., F.-F. Jin, and J.-S. Kug, 2014: Eddy-induced growth rate of low-frequency
 570 variability and its mid-to late winter suppression in the Northern Hemisphere, *J. Atmos. Sci.*,
 571 **71**, 2281–2298.

572 Ren, X., X. Yang, and C. Chu, 2010: Seasonal variations of the synoptic-scale transient eddy
 573 activity and polar front jet over east asia, *J. Climate*, **23** , 3222–3233.

574 D.P. Robinson, D.P., R.X. Black, and B.A. McDaniel, 2006: A Siberian precursor to midwinter
 575 intraseasonal variability in the North Pacific storm track. *Geophys. Res. Lett.*, **33**, L15811,
 576 doi:10.1029/2006GL026458

577 Serreze, M.C., J.E. Box, R.G. Barry and J.E. Walsh, 1993: Characteristics of Arctic synoptic
 578 activity. *Meteor. Atmos. Phys.*, **51**, 147-164.

579 Serreze M. C. and A. P. Barrett, 2008: The summer cyclone maximum over the Central Arctic
 580 Ocean, *J. Climate*, **21**, 1048–1065.

581 Schemm, S., and T. Schneider, 2018: **Eddy lifetime, number, and diffusivity and the suppression of**
 582 **eddy kinetic energy in midwinter**. *Journal of Climate*, **31**, 5649-5665.

583 Simpson, R. H., 1952: Evolution of the Kona storm: A subtropical cyclone. *J. Meteorol.*, **9**, 24-
 584 35.

585 Thorncroft, C. D., and K. Hodges, 2001: African easterly wave variability and its relationship
 586 to Atlantic tropical cyclone activity. *J. Climate*, **14**, 1166–1179.

587 Tian, S.F., and T. Yasanari, 1998: Climatological aspects and mechanism of the spring
588 persistent rains over central China. *J. Meteorol. Soc. Japan*, **76**, 57-71.

589 Trigo, I. F., T. D. Davies, G. R. Bigg, 1999: Objective climatology of cyclones in the
590 Mediterranean Region, *J. Clim.*, **12**, 1685–1696.

591 Woollings, T., A. Hannachi, and B. Hoskins, 2010: Variability of the North Atlantic eddy-
592 driven jet stream. *Q. J. R. Meteorol. Soc.*, **136**, 856–868. doi:10.1002/qj.625.

593 Zhang X., J. E. Walsh, J. Zhang, U. S. Bhatt and M. Ikeda , 2004: Climatology and interannual
594 variability of arctic cyclone activity: 1948–2002, *J. Clim.*, **17**, 2300–2317.

595

Captions

Figure 1. Track density (contours) and mean intensity (colour) for tracking of maxima in the modulus of the meridional wind at 850hPa, $|V_{850}|$, for the winter season, DJF, with the sectors considered in this study delineated by black lines for the main sectors discussed in the text and yellow lines for the sectors shown in the supplementary material. Track density contours are every 5 with the dashed line at 12.5 in units of number per month per unit area, where the unit area is equivalent to a 5° spherical cap, $\sim (10^3 \text{ km})^2$. The intensity is in units of m s^{-1} . Mean intensity is suppressed for track densities below 1.0.

Figure 2. The storm-track in the Central Pacific (CP) sector as a function of the time of year and latitude. The 250hPa and 850hPa levels are shown in the upper (a, b) and lower (c, d) panels, respectively. The left column (a, c) is for the standard deviation (SD) of the meridional wind (V), with (a) overlaid with $U_{PV=2}$ (contours starting at 20ms^{-1} and interval 10ms^{-1}) and (c) overlaid with U_{850} (contours at 5ms^{-1} and 10ms^{-1}). The right column (b, d) show tracking statistics for $|V|$ maxima, and show track density (lines, ci of 2.0, long dashed lines are 10.0 and short dashed lines are 20.0) and mean intensity (colour). The units for SD and intensity are ms^{-1} and for track density the number per month per unit area, where the unit area is equivalent to a 5° spherical cap, $\sim (10^3 \text{ Km})^2$.

Figure 3. Summaries of the annual cycle of the storm-track maxima in the Central Pacific (CP) sector. The 250hPa and 850hPa levels are shown in the upper (a, b) and lower (c, d) panels, respectively. The left column (a, c) is for the standard deviation (SD) of the meridional wind (V) and shows for each month the latitude of the maximum and its magnitude. The right column (b, d) is for tracking fields for $|V|$ maxima, and shows for each month the latitude of the track density maximum and the mean intensity at that latitude.

619 The units of SD and intensity are m s^{-1} . The colour coding for the months is shown in (b), and
620 the consecutive months from January to December are joined by straight lines.

621 Figure 4. The storm-track in the Western Pacific (WP) sector as a function of the time of year
622 and latitude. The 250hPa and 850hPa levels are shown in the upper (a, b) and lower (c, d)
623 panels, respectively. The left column (a, c) is for the standard deviation (SD) of the
624 meridional wind (V) with (a) overlaid with $U_{PV=2}$ (contours starting at 20ms^{-1} and interval
625 10ms^{-1}) and (c) overlaid with U_{850} (contours at 5ms^{-1} and 7.5ms^{-1} (dashed)). The right
626 column (b, d) is for tracking statistics for $|V|$ maxima, and show track density (lines) and
627 mean intensity (colour). The conventions are as in Fig.2.

628 Figure 5. The storm-track in the Eastern Pacific (EP) sector as a function of the time of year
629 and latitude. The 250hPa and 850hPa levels are shown in the upper (a, b) and lower (c, d)
630 panels, respectively. The left column (a, c) is for the standard deviation (SD) of the
631 meridional wind (V) with (a) overlaid with $U_{PV=2}$ (contours at 15 (dashed), 20, and 25ms^{-1}
632 (dashed)) and (c) overlaid with U_{850} (contours at 5ms^{-1} and 7.5ms^{-1} (dashed)). The right
633 column (b, d) is for tracking fields for $|V|$ maxima, and show track density (lines) and mean
634 intensity (colour). The conventions are as in Fig.2.

635 Figure 6. Summaries of the annual cycle of the storm-track maxima in the Eastern Pacific
636 (EP) sector. The 250hPa and 850hPa levels are shown in the upper (a, b) and lower (c, d)
637 panels, respectively. The left column (a, c) is for the standard deviation (SD) of the
638 meridional wind (V) and shows for each month the latitude of the maximum and its
639 magnitude. The right column (b, d) is for tracking fields for $|V|$ maxima, and shows for each
640 month the latitude of the track density maximum and the mean intensity at that latitude.
641 The conventions are as in Fig. 3.

Figure 7. The storm-track in the Western Atlantic (WA) sector as a function of the time of year and latitude. The 250hPa and 850hPa levels are shown in the upper (a, b) and lower (c, d) panels, respectively. The left column (a, c) is for the standard deviation (SD) of the meridional wind (V) with (a) overlaid with $U_{PV=2}$ (contours starting at 20ms^{-1} and interval 10ms^{-1}) and (c) overlaid with U_{850} (contours at 5, 7.5 (dashed), and 10ms^{-1}). The right column (b, d) are the tracking statistics for $|V|$ maxima, and show track density (lines) and mean intensity (colour). The conventions are as in Fig.2.

Figure 8. Summaries of the annual cycle of the storm-track maxima in the Western Atlantic (WA) sector. The 250hPa and 850hPa levels are shown in the upper (a, b) and lower (c, d) panels, respectively. The left column (a, c) is for the standard deviation (SD) of the meridional wind (V) and shows for each month the latitude of the maximum and its magnitude. The right column (b, d) is for tracking fields for $|V|$ maxima, and shows for each month the latitude of the track density maximum and the mean intensity at that latitude. The conventions are as in Fig. 3.

Figure 9. The storm-track in the Central Atlantic (CA) sector as a function of the time of year and latitude. The 250hPa and 850hPa levels are shown in the upper (a, b) and lower (c, d) panels, respectively. The left column (a, c) is for the standard deviation (SD) of the meridional wind (V) with (a) overlaid with $U_{PV=2}$ (contours starting at 20ms^{-1} and interval 10ms^{-1}) and (c) overlaid with U_{850} (contours at 5, 7.5 (dashed), and 10ms^{-1}). The right column (b, d) shows the tracking statistics for $|V|$ maxima, and show track density (lines) and mean intensity (colour). The conventions are as in Fig.2.

Figure 10. The storm-track in the Eastern Atlantic (EA) sector as a function of the time of year and latitude. The 250hPa and 850hPa levels are shown in the upper (a, b) and lower (c,

665 d) panels, respectively. The left column (a, c) is for the standard deviation (SD) of the
666 meridional wind (V) with (a) overlaid with $U_{PV=2}$ (contours at 15 (dashed), 20, and 30ms^{-1})
667 and (c) overlaid with U_{850} (contours at 5 and 7.5ms^{-1} (dashed)). The right column (b, d) is
668 for tracking fields for $|V|$ maxima, and show track density (lines) and mean intensity
669 (colour). The conventions are as in Fig.2.

670

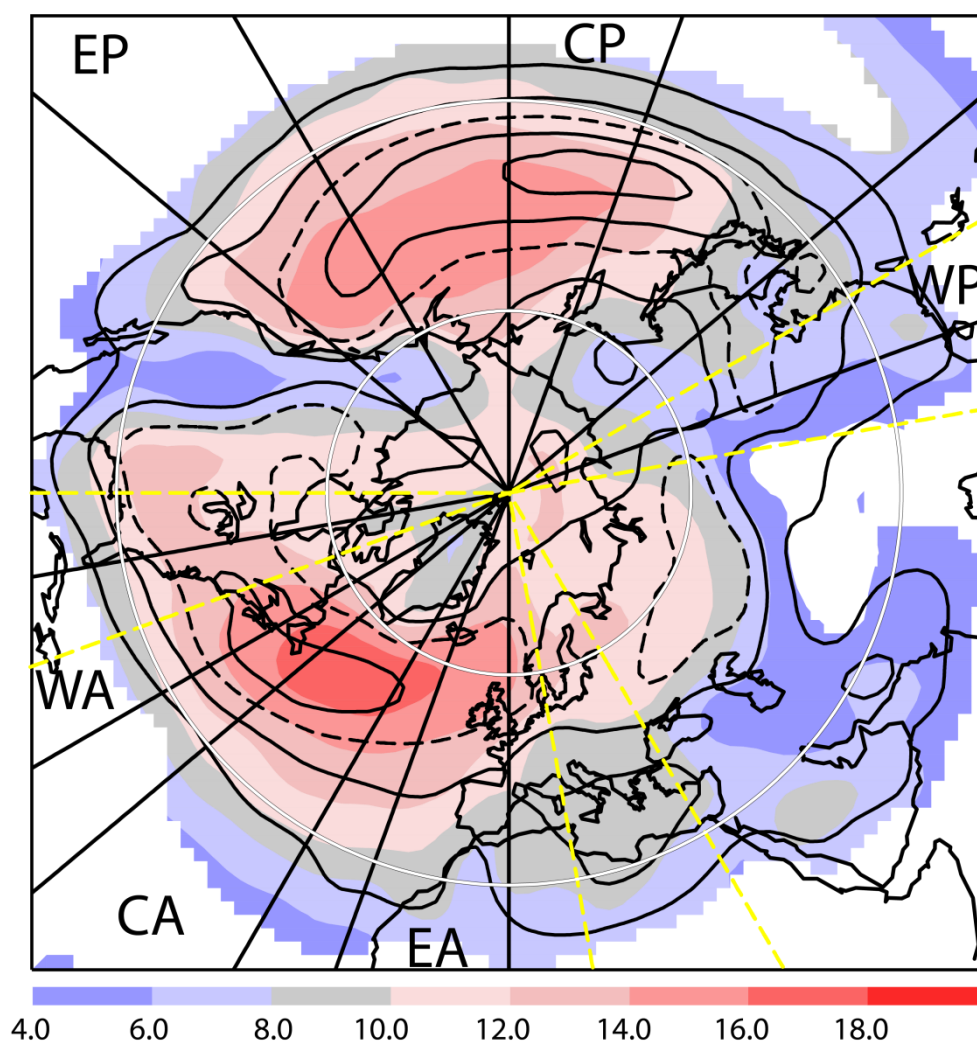


Figure 1. Track density (contours) and mean intensity (colour) for tracking of maxima in the modulus of the meridional wind at 850hPa, $|V_{850}|$, for the winter season, DJF, with the sectors considered in this study delineated by black lines for the main sectors discussed in the text and yellow lines for the sectors shown in the supplementary material. Track density contours are every 5 with the dashed line at 12.5 in units of number per month per unit area, where the unit area is equivalent to a 5° spherical cap, $\sim (10^3 \text{ km})^2$. The intensity is in units of m s^{-1} . Mean intensity is suppressed for track densities below 1.0.

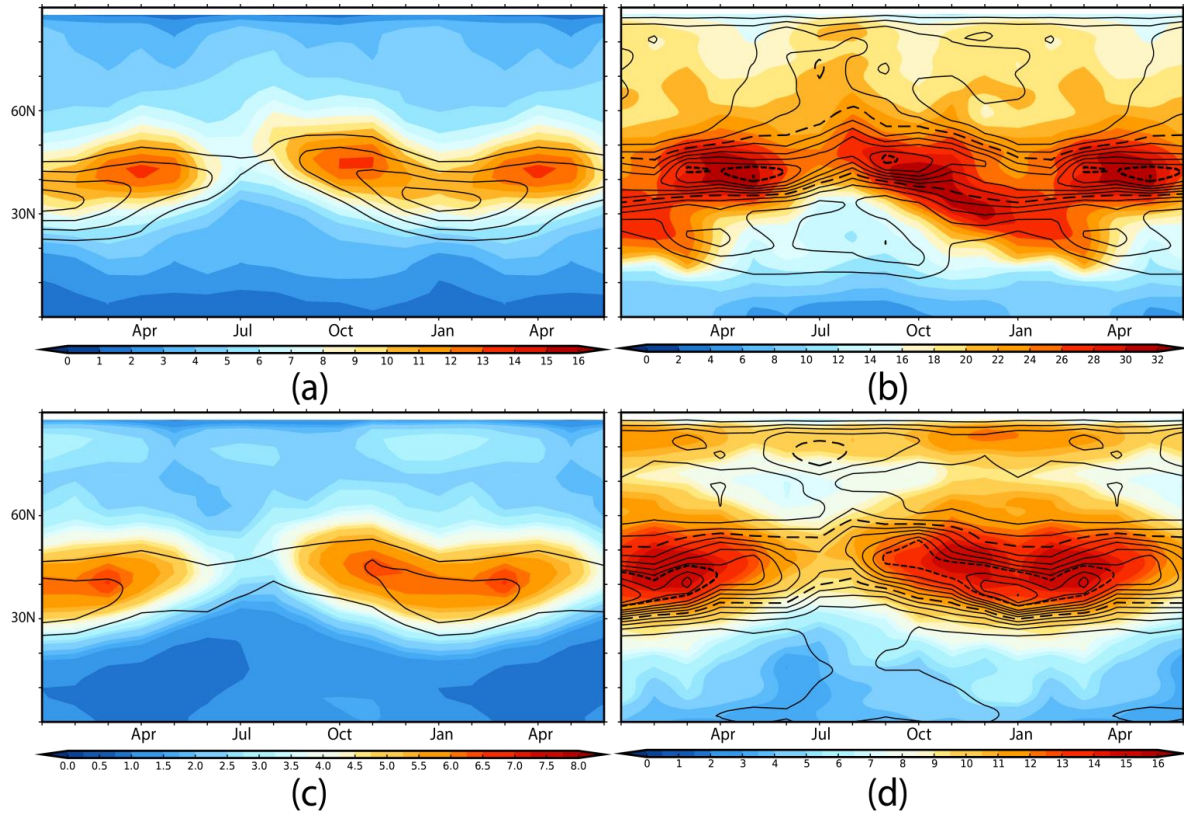


Figure 2. The storm-track in the Central Pacific (CP) sector as a function of the time of year and latitude. The 250hPa and 850hPa levels are shown in the upper (a, b) and lower (c, d) panels, respectively. The left column (a, c) is for the standard deviation (SD) of the meridional wind (V), with (a) overlaid with $U_{PV=2}$ (contours starting at 20ms^{-1} and interval 10ms^{-1}) and (c) overlaid with U_{850} (contours at 5ms^{-1} and 10ms^{-1}). The right column (b, d) show tracking statistics for $|V|$ maxima, and show track density (lines, ci of 2.0, long dashed lines are 10.0 and short dashed lines are 20.0) and mean intensity (colour). The units for SD and intensity are ms^{-1} and for track density the number per month per unit area, where the unit area is equivalent to a 5° spherical cap, $\sim (10^3 \text{ Km})^2$.

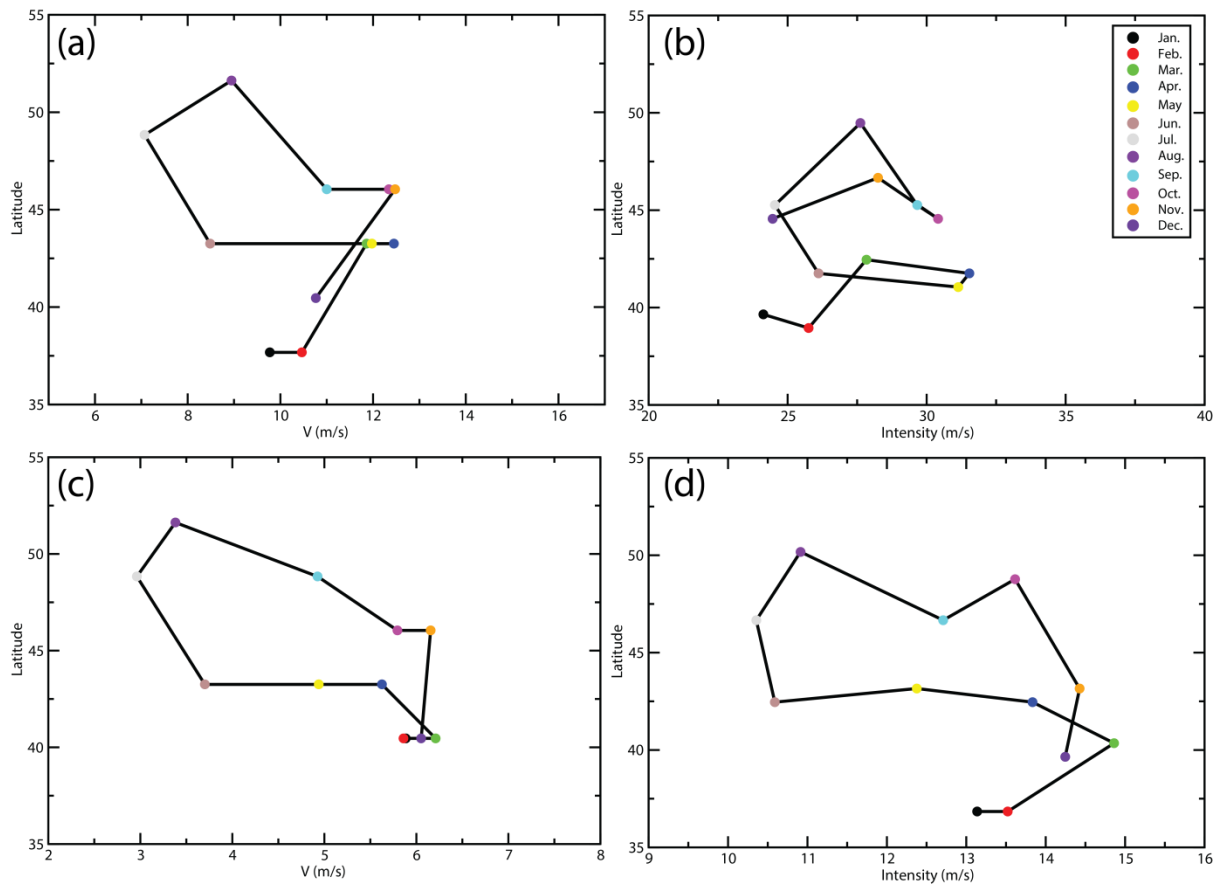


Figure 3. Summaries of the annual cycle of the storm-track maxima in the Central Pacific (CP) sector. The 250hPa and 850hPa levels are shown in the upper (a, b) and lower (c, d) panels, respectively. The left column (a, c) is for the standard deviation (SD) of the meridional wind (V) and shows for each month the latitude of the maximum and its magnitude. The right column (b, d) is for tracking fields for $|V|$ maxima, and shows for each month the latitude of the track density maximum and the mean intensity at that latitude. The units of SD and intensity are m s^{-1} . The colour coding for the months is shown in (b), and the consecutive months from January to December are joined by straight lines.

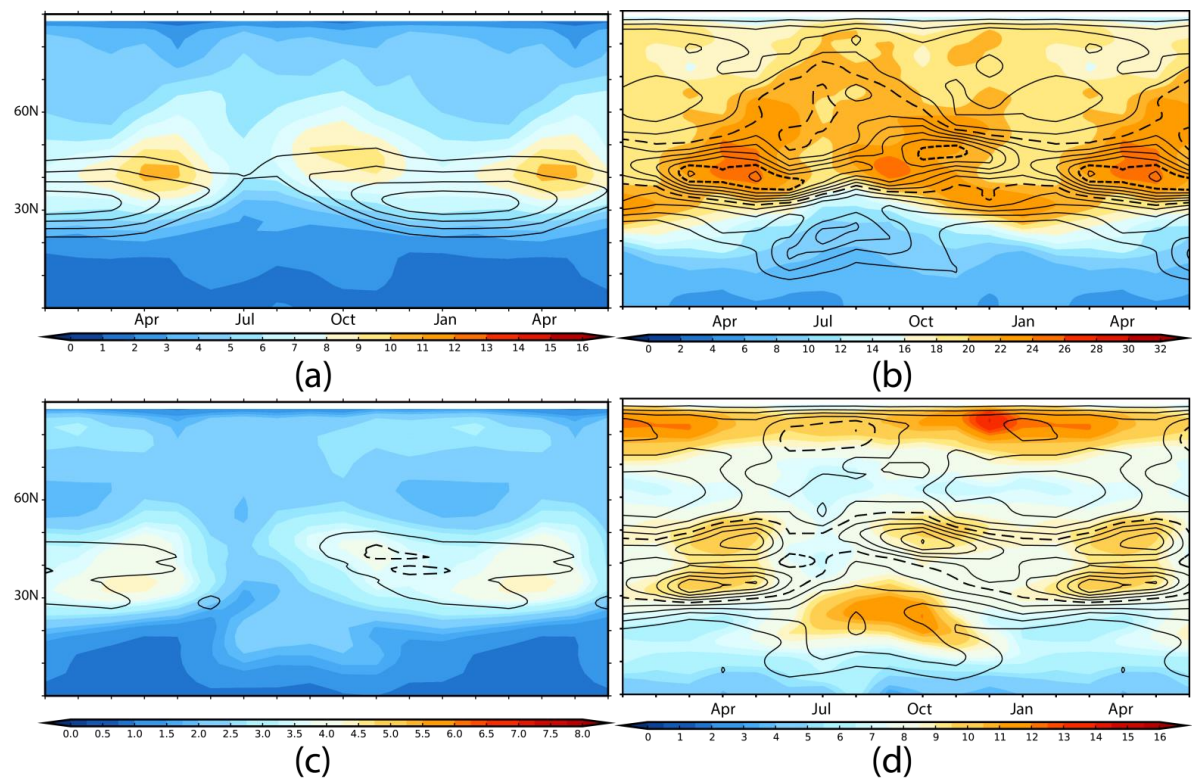
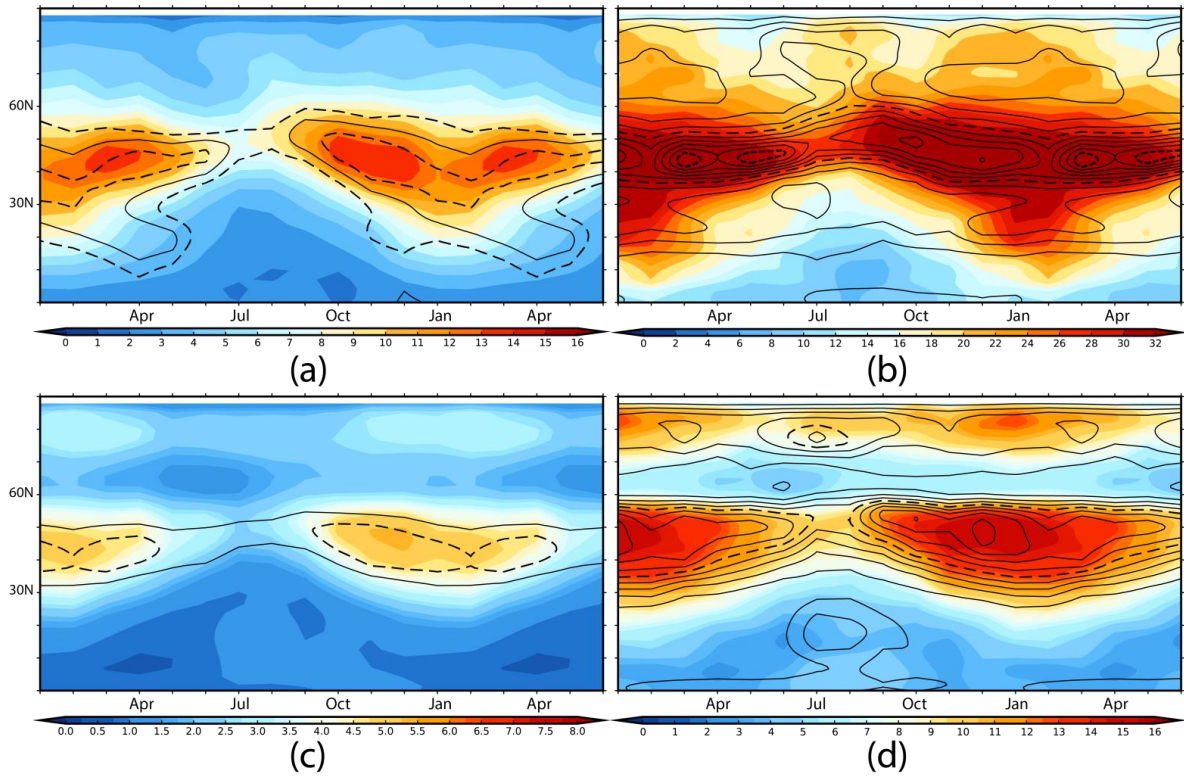


Figure 4. The storm-track in the Western Pacific (WP) sector as a function of the time of year and latitude. The 250hPa and 850hPa levels are shown in the upper (a, b) and lower (c, d) panels, respectively. The left column (a, c) is for the standard deviation (SD) of the meridional wind (V) with (a) overlaid with $U_{PV=2}$ (contours starting at 20ms^{-1} and interval 10ms^{-1}) and (c) overlaid with U_{850} (contours at 5ms^{-1} and 7.5ms^{-1} (dashed)). The right column (b, d) is for tracking statistics for $|V|$ maxima, and show track density (lines) and mean intensity (colour). The conventions are as in Fig.2.



714

715

716

717

718

719

720

721

722

Figure 5. The storm-track in the Eastern Pacific (EP) sector as a function of the time of year and latitude. The 250hPa and 850hPa levels are shown in the upper (a, b) and lower (c, d) panels, respectively. The left column (a, c) is for the standard deviation (SD) of the meridional wind (V) with (a) overlaid with $U_{PV=2}$ (contours at 15 (dashed), 20, and 25 ms^{-1} (dashed)) and (c) overlaid with U_{850} (contours at 5 ms^{-1} and 7.5 ms^{-1} (dashed)). The right column (b, d) is for tracking fields for $|V|$ maxima, and show track density (lines) and mean intensity (colour). The conventions are as in Fig.2.

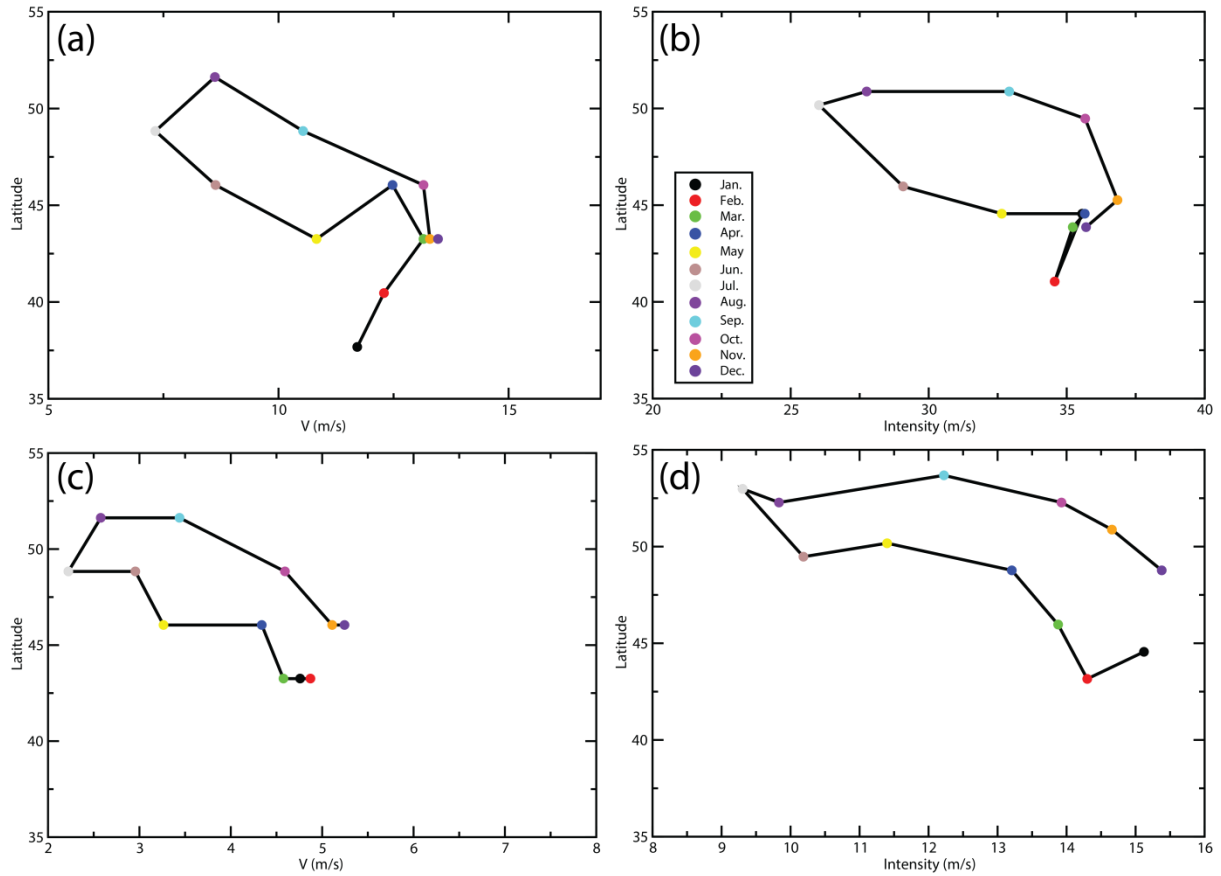
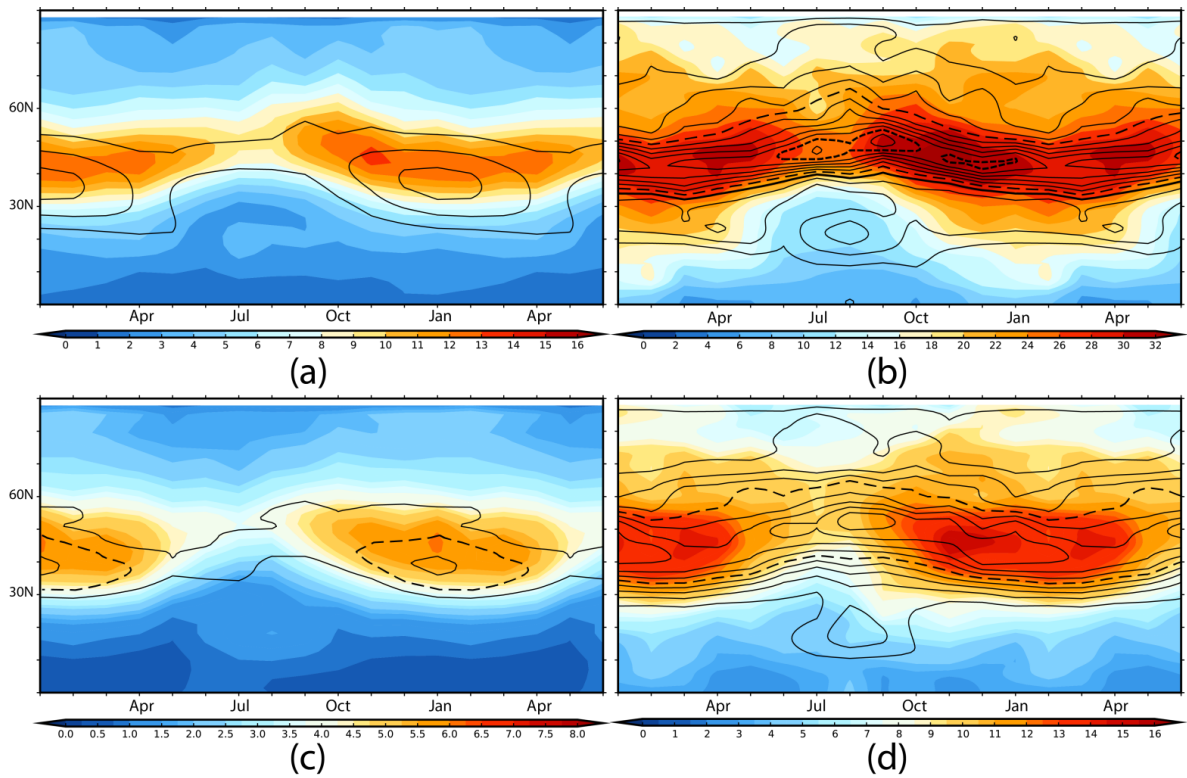


Figure 6. Summaries of the annual cycle of the storm-track maxima in the Eastern Pacific (EP) sector. The 250hPa and 850hPa levels are shown in the upper (a, b) and lower (c, d) panels, respectively. The left column (a, c) is for the standard deviation (SD) of the meridional wind (V) and shows for each month the latitude of the maximum and its magnitude. The right column (b, d) is for tracking fields for $|V|$ maxima, and shows for each month the latitude of the track density maximum and the mean intensity at that latitude. The conventions are as in Fig. 3.



732

733

734

735

736

737

738

739

Figure 7. The storm-track in the Western Atlantic (WA) sector as a function of the time of year and latitude. The 250hPa and 850hPa levels are shown in the upper (a, b) and lower (c, d) panels, respectively. The left column (a, c) is for the standard deviation (SD) of the meridional wind (V) with (a) overlaid with $U_{PV=2}$ (contours starting at 20ms^{-1} and interval 10ms^{-1}) and (c) overlaid with U_{850} (contours at 5, 7.5 (dashed), and 10ms^{-1}). The right column (b, d) are the tracking statistics for $|V|$ maxima, and show track density (lines) and mean intensity (colour). The conventions are as in Fig.2.

740

741

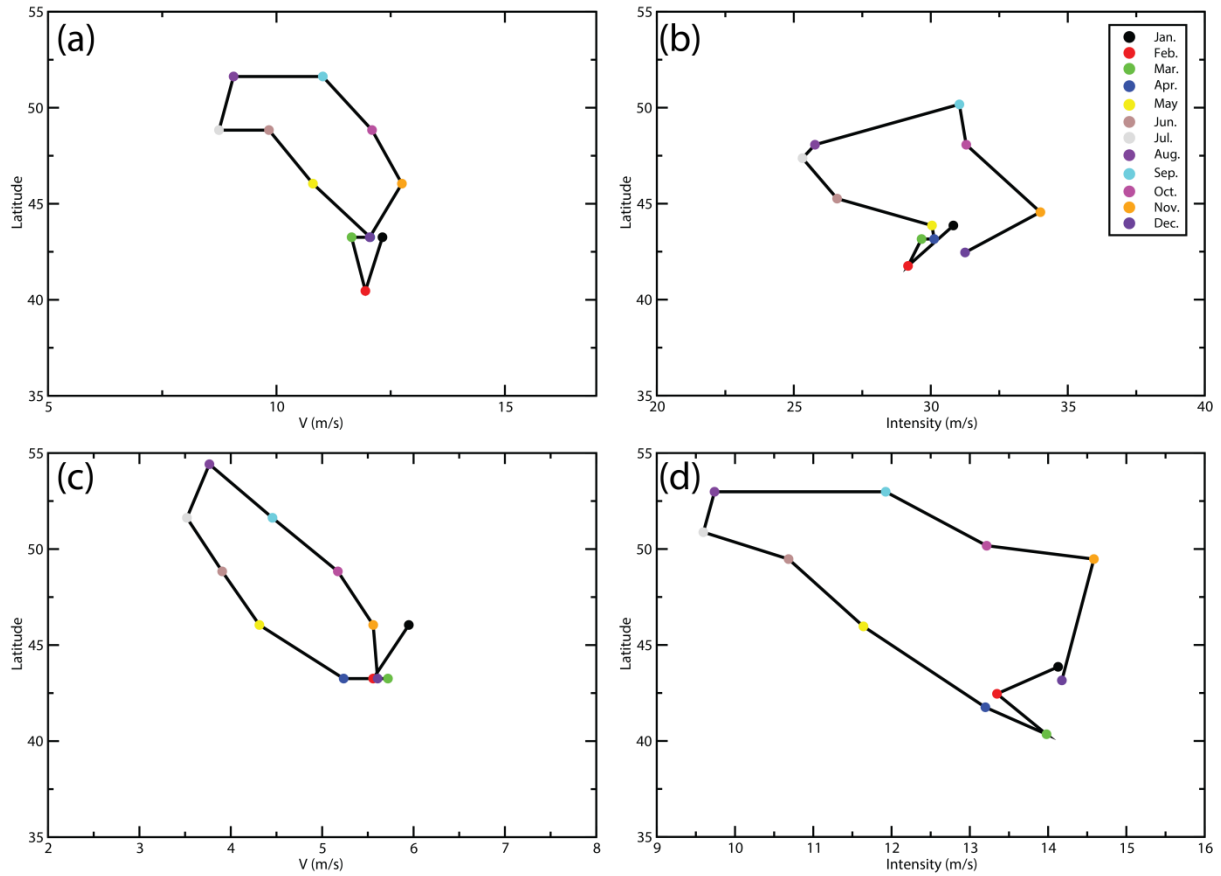
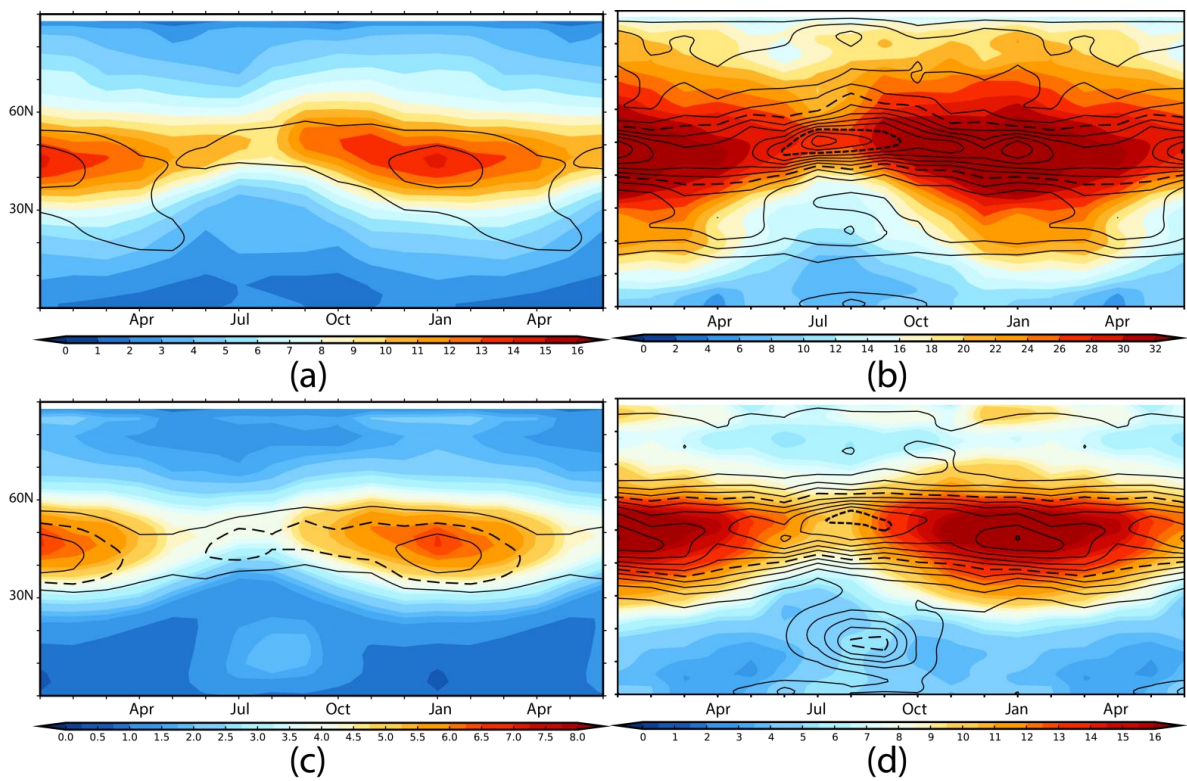


Figure 8. Summaries of the annual cycle of the storm-track maxima in the Western Atlantic (WA) sector. The 250hPa and 850hPa levels are shown in the upper (a, b) and lower (c, d) panels, respectively. The left column (a, c) is for the standard deviation (SD) of the meridional wind (V) and shows for each month the latitude of the maximum and its magnitude. The right column (b, d) is for tracking fields for $|V|$ maxima, and shows for each month the latitude of the track density maximum and the mean intensity at that latitude. The conventions are as in Fig. 3.

751



752

753

754

755

756

757

758

759

Figure 9. The storm-track in the Central Atlantic (CA) sector as a function of the time of year and latitude. The 250hPa and 850hPa levels are shown in the upper (a, b) and lower (c, d) panels, respectively. The left column (a, c) is for the standard deviation (SD) of the meridional wind (V) with (a) overlaid with $U_{PV=2}$ (contours starting at 20ms^{-1} and interval 10ms^{-1}) and (c) overlaid with U_{850} (contours at 5, 7.5 (dashed), and 10ms^{-1}). The right column (b, d) shows the tracking statistics for $|V|$ maxima, and show track density (lines) and mean intensity (colour). The conventions are as in Fig.2.

760

761

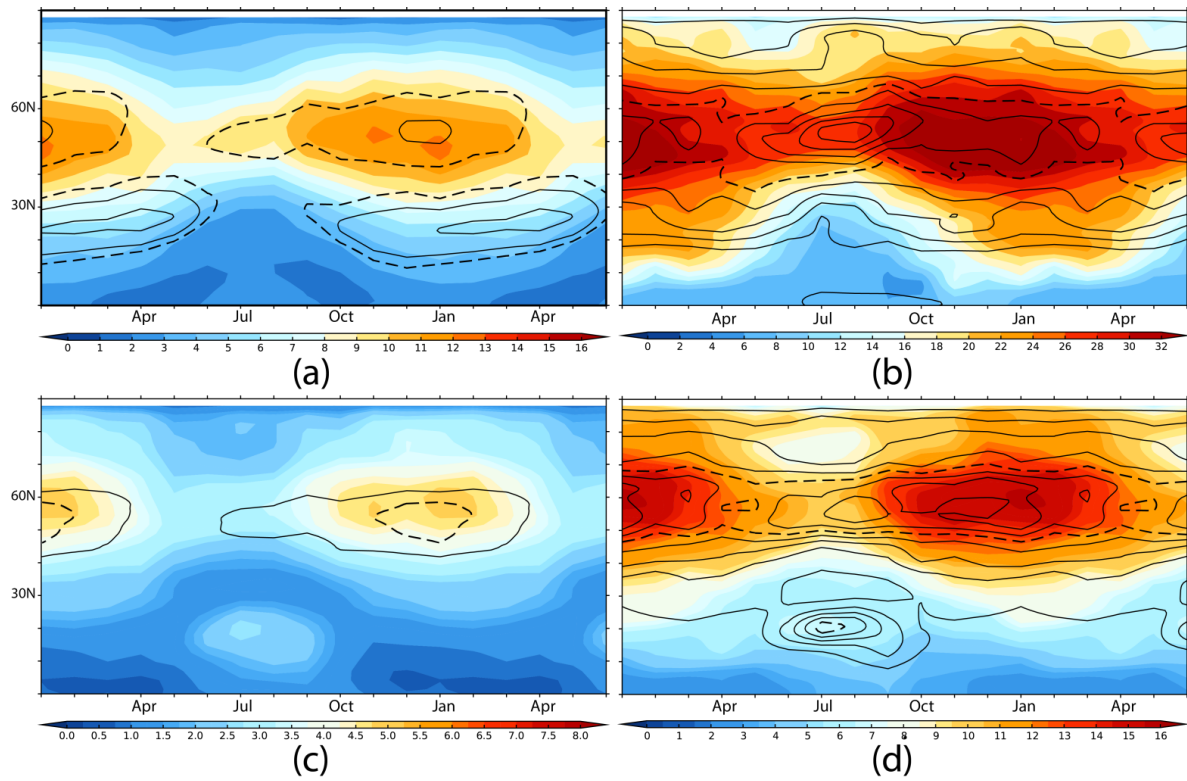


Figure 10. The storm-track in the Eastern Atlantic (EA) sector as a function of the time of year and latitude. The 250hPa and 850hPa levels are shown in the upper (a, b) and lower (c, d) panels, respectively. The left column (a, c) is for the standard deviation (SD) of the meridional wind (V) with (a) overlaid with $U_{PV=2}$ (contours at 15 (dashed), 20, and 30 ms^{-1}) and (c) overlaid with U_{850} (contours at 5 and 7.5 ms^{-1} (dashed)). The right column (b, d) is for tracking fields for $|V|$ maxima, and show track density (lines) and mean intensity (colour). The conventions are as in Fig.2.